Plane Waves in FDTD Simulations and a Nearly Perfect Total-Field/Scattered-Field Boundary

John B. Schneider, *Member, IEEE*

***Abstract*—The total-field/scattered-field (TFSF) boundary has been successfully used for a number of years to introduce energy into finite-difference time-domain (FDTD) grids. If the propagation of the incident field is grid-aligned, a perfect TFSF implementation can be realized by using an auxiliary one-dimensional FDTD simulation which models propagation of the incident field. Here "perfect" implies the incident field propagation exactly matches the way in which the field propagates in the FDTD grid. However, for propagation which is not grid-aligned, no similarly perfect implementation has previously been presented. This work provides a framework for a perfect TFSF boundary for pulsed plane waves which do not propagate in a grid-aligned fashion. To achieve this, homogeneous plane-wave propagation is rigorously quantified. Using this knowledge and a specification of the desired incident field, the dispersion relation is used to ascertain the incident field at any point in the grid. It is required to account for, unlike in the continuous world, the electric field, the magnetic field, and the wavenumber vector not forming a mutually orthogonal set. Group velocity is also considered because of its relevance to the implementation.**

***Index Terms*—Finite-difference time-domain (FDTD) methods.**

I. Introduction

THE total-field/scattered-field (TFSF) boundary formulation, first described in [1] in terms of Huygen's surfaces, provides a relatively simple method for introducing arbitrary incident fields into finite-difference time-domain (FDTD) grids. A detailed discussion of the implementation of TFSF boundaries for pulsed plane waves can be found in [2], [3]. The framework presented here will use the context of the standard Yee FDTD scheme [4] although the same concepts should apply equally well to any scheme for which the dispersion relation is known exactly. TFSF boundaries have recently been adapted to work when partially embedded within a perfectly matched layer [5]. It is also possible to apply the TFSF concept to stratified media as shown in [6]. In this work the boundary is assumed to lie in a homogeneous medium (which may enclose an arbitrary scatterer) and the incident field is a pulsed plane wave.

The TFSF boundary is a fictitious boundary which encloses a portion of the computational domain. Nodes inside the boundary are in the total-field (TF) region, i.e., incident field plus any scattered field, and nodes outside it are in the scattered-field (SF) region. The TFSF boundary works by adjusting the value of nodes adjacent to the boundary, i.e., nodes whose neighboring nodes lie on the other side of the boundary. For a total-field node adjacent to the boundary, one or more neighboring nodes lack the incident field. When applying the update equation to this TF node, the incident field must be added to the neighbors which lack it in order to get a consistent equation. On the other hand, when updating a scattered-field node, the incident field must be subtracted from neighbors which lie in the TF region (see [2], [3] for implementation details).

One must specify the incident field at all the electric and magnetic field nodes adjacent to the TFSF boundary. If one uses the analytic form for the incident field (i.e., the one which describes propagation in the continuous world), numerical artifacts will be introduced since the way in which the fields propagate in the FDTD grid differs from how they propagate in the continuous world. Since all propagating waves in the FDTD grid travel slower than in the continuous world, this mismatch will cause fields to leak across the boundary. This leakage can be reduced by using a finer discretization, but it cannot be eliminated. A simple and elegant way to overcome this problem for grid-aligned propagation is to use a one-dimensional (1-D) auxiliary FDTD computation to model the propagation of the incident field [2], [3]. By using the same parameters (i.e., spatial-step size in the direction of propagation, temporal-step size, Courant number, etc.) in the 1-D grid and the grid in which the TFSF boundary is to be realized, one can ensure that the incident field given by the 1-D grid exactly matches how the incident field propagates in the other grid. Thus, for grid-aligned propagation there will be no leakage across the boundary.

Unfortunately when propagation is not grid-aligned, it is not possible to model exactly the way the field propagates in the higher-dimensional grid using a 1-D grid. One correction, proposed in [2], [3], adjusts the phase velocity in the 1-D auxiliary grid so that a single spectral component will match the phase velocity in the higher-dimensional grid. This correction might be done at the frequency component corresponding to the most energetic spectral component of the pulse or some other frequency which is of particular interest. However, the phase velocity would only be correct at that single frequency. All other spectral components would be subject to leakage across the boundary. Another scheme for using a 1-D auxiliary grid was proposed by Guiffaut and Mahdjoubi [7]. In their approach the auxiliary grid uses the same temporal-step size and speed of propagation as the higher-dimensional grid but the spatial-step size is chosen to ensure the phase speeds are matched at some suitable discretization. Despite the title of their work, Guiffaut and Mahdjoubi's scheme does have inherent approximations—the phase velocities are not exactly the same

Manuscript received January 16, 2004. This work was supported by the Office of Naval Research Code 321OA.

The author is with the School of Electrical Engineering and Computer Science, Washington State University, Pullman, WA 99164-2752 USA (e-mail: schneidj@eecs.wsu.edu).

Digital Object Identifier 10.1109/TAP.2004.836403

in the two grids (although they are indeed very close for most practical discretizations).

If one chooses to use a 1-D auxiliary-grid scheme, one must interpolate the fields of the 1-D grid to points corresponding to the projected locations of the nodes in the higher-dimensional grid. This interpolation comes with its own set of artifacts which has been addressed in [8] and [9]. Additionally, to date, no TFSF scheme has accounted for the fact that for nongrid-aligned propagation of a homogeneous plane wave, the electric field, the magnetic field, and the direction of propagation (i.e., the wavenumber vector) do not form a mutually orthogonal set (as they do in the continuous world). Failure to account for this can introduce additional numeric artifacts.

This work attempts to provide a framework which is perfect (or in which the errors can be made arbitrarily small without resorting to a smaller discretization). Perfect should not be taken to mean corresponding to the continuous-world but rather we seek a way to obtain the exact incident field as would be found at an arbitrary point in the FDTD grid without performing an FDTD simulation. For the sake of implementation, some compromises will be made (and noted accordingly). The exact scheme starts with an incident angle, a specified incident time series, and a reference point at which that time series is assumed to exist. Then the dispersion relation [10] is used to obtain a time series at an arbitrary point in the FDTD space (incidently, this point does not have to correspond to an actual grid node). In this way it is possible to specify exactly what the incident field should be, in the time domain, at any node in the grid. The use of the dispersion relation to describe propagation of a pulsed field in FDTD grids, without actually doing an FDTD simulation, was discussed in [11]. The dispersion relation was further explored in [12] where it was speculated that it would be possible to construct a perfect TFSF boundary. Missing from those two papers was consideration of the nonorthogonality of the fields and the wavenumber vector. This issue was explored in [13] and had been considered previously by Celuch-Marcysiak and Gwarek [14] in the context of the divergence properties of FDTD schemes.

The technique presented here does not necessarily claim to be faster than previously proposed 1-D auxiliary schemes (but does make the claim of significantly improved accuracy). Nevertheless, the code written to realize the perfect TFSF boundary is very fast and employs the FFTw software suite (i.e., Fastest Fourier Transform in the West, [15] or see www.fftw.org for further details). The code permits the *a priori* calculation of the fields adjacent to the TFSF boundary so that they can be stored in a data file and read during an FDTD simulation (and used multiple times if desired). Alternatively, another version of the code is designed for incorporation directly into the main FDTD code where a single function call initializes the incident fields and then one other function is called at each time step to perform the necessary operations on fields adjacent to the TFSF boundary.

The following section provides the necessary background material to construct the exact TFSF boundary. Section III presents implementation details. Results are given in Section IV and finally conclusions are presented in Section V.

II. Background

It is necessary to quantify rigorously the way in which plane waves, which are eigen functions of the FDTD method, propagate in the grid. To this end we adopt the notation developed by Forgy [16]. The electric and magnetic fields are given by

$$\hat{\mathbf{E}}^{\mathbf{m}} = \hat{\mathbf{E}}_0 e^{j(\omega m_t \Delta_t - \tilde{k}_x m_x \Delta_x - \tilde{k}_y m_y \Delta_y - \tilde{k}_z m_z \Delta_z)} \tag{1}$$

$$\hat{\mathbf{H}}^{\mathbf{m}} = \hat{\mathbf{H}}_0 e^{j(\omega m_t \Delta_t - \tilde{k}_x m_x \Delta_x - \tilde{k}_y m_y \Delta_y - \tilde{k}_z m_z \Delta_z)} \tag{2}$$

where, for a plane wave propagating at an angle of θ relative to the z axis and the angle ϕ relative to the x axis when projected in the xy plane, the numeric wavenumber vector $\tilde{\mathbf{k}}$ is given by

$$\tilde{\mathbf{k}} = [\tilde{k}_x, \tilde{k}_y, \tilde{k}_z] = \tilde{k}[\sin\theta\cos\phi, \sin\theta\sin\phi, \cos\theta] \tag{3}$$

the vector $\mathbf{m} = [m_t, m_x, m_y, m_z]$ gives the temporal and spatial indices of a node, Δ_t is the temporal-step size, $\Delta_i\, i \in \{x, y, z\}$ are the spatial-step sizes, and ω is the frequency. The vectors $\hat{\mathbf{E}}_0$ and $\hat{\mathbf{H}}_0$ are constant for any given frequency. A tilde will be used to indicate a numeric quantity, i.e., one that exists in the FDTD grid and which typically differs from its corresponding value in the continuous world. A caret over an electric or magnetic field implies it is in the frequency domain. Let the shift operator s_i^+ shift the ith index by $+1/2$. For example

$$s_x^+ \hat{\mathbf{E}}^{[m_t, m_x, m_y, m_z]} = \hat{\mathbf{E}}^{[m_t, m_x + 1/2, m_y, m_z]}. \tag{4}$$

Conversely, s_i^- shifts the ith index by $-1/2$. The discrete differential operator $\tilde{\partial}_i$ is defined as

$$\tilde{\partial}_i = \frac{1}{\Delta_i}(s_i^+ - s_i^-). \tag{5}$$

Using this notation, the Yee FDTD version of Ampere's and Faraday's equations can be stated succinctly as

$$\bar{\mathbf{S}}^+ s_t^+ \tilde{\partial}_t \epsilon \hat{\mathbf{E}}^{\mathbf{m}} = \bar{\mathbf{S}}^+ s_t^+ \tilde{\nabla} \times \hat{\mathbf{H}}^{\mathbf{m}} \tag{6}$$

$$-\bar{\mathbf{S}}^- s_x^+ s_y^+ s_z^+ \tilde{\partial}_t \mu \hat{\mathbf{H}}^{\mathbf{m}} = \bar{\mathbf{S}}^- s_x^+ s_y^+ s_z^+ \tilde{\nabla} \times \hat{\mathbf{E}}^{\mathbf{m}} \tag{7}$$

where the shift matrix $\bar{\mathbf{S}}^+$ is given by

$$\bar{\mathbf{S}}^+ = \begin{bmatrix} s_x^+ & 0 & 0 \\ 0 & s_y^+ & 0 \\ 0 & 0 & s_z^+ \end{bmatrix} \tag{8}$$

while $\bar{\mathbf{S}}^-$ uses negative shift operators along the diagonal, and the discrete nabla operator is defined as the vector $\tilde{\nabla} = [\tilde{\partial}_x, \tilde{\partial}_y, \tilde{\partial}_z]$. For plane-wave propagation the discrete differential operators become

$$\tilde{\partial}_i \hat{\mathbf{E}}^{\mathbf{m}} = -j\frac{2}{\Delta_i}\sin\left(\frac{\tilde{k}_i \Delta_i}{2}\right)\hat{\mathbf{E}}^{\mathbf{m}}, \quad i \in \{x, y, z\} \tag{9}$$

$$\tilde{\partial}_t \hat{\mathbf{E}}^{\mathbf{m}} = j\frac{2}{\Delta_t}\sin\left(\frac{\omega \Delta_t}{2}\right)\hat{\mathbf{E}}^{\mathbf{m}}. \tag{10}$$

We define K_i and Ω as

$$K_i = \frac{2}{\Delta_i}\sin\left(\frac{\tilde{k}_i \Delta_i}{2}\right), \quad i \in \{x, y, z\} \tag{11}$$

$$\Omega = \frac{2}{\Delta_t}\sin\left(\frac{\omega \Delta_t}{2}\right) \tag{12}$$

so that for a plane wave the discrete nabla operator is given by $\tilde{\nabla} = -j[K_x, K_y, K_z] = -j\mathbf{K}$.

A. Non-Orthogonality of $\hat{\mathbf{E}}^{\mathbf{m}}, \hat{\mathbf{H}}^{\mathbf{m}}$, and $\tilde{\mathbf{k}}$

In a source-free region, it can be shown that the Yee grid is identically divergence free [2], [3]. Hence

$$\tilde{\nabla} \cdot \hat{\mathbf{E}}^{\mathbf{m}} = 0 \Leftrightarrow -j\mathbf{K} \cdot \hat{\mathbf{E}}^{\mathbf{m}} = 0 \tag{13}$$

$$\tilde{\nabla} \cdot \hat{\mathbf{H}}^{\mathbf{m}} = 0 \Leftrightarrow -j\mathbf{K} \cdot \hat{\mathbf{H}}^{\mathbf{m}} = 0. \tag{14}$$

Equation (13) dictates that $\mathbf{K}$ and the electric field are orthogonal while (14) requires $\mathbf{K}$ and the magnetic field to be orthogonal. Additionally, the curl operator can be expressed in terms of $\mathbf{K}$. Returning to the Yee algorithm given by (6) and (7), canceling the shift operators, and substituting the plane-wave form of the differential operators, one obtains

$$j\Omega\epsilon\hat{\mathbf{E}}^{\mathbf{m}} = -j\mathbf{K} \times \hat{\mathbf{H}}^{\mathbf{m}} \tag{15}$$

$$-j\Omega\mu\hat{\mathbf{H}}^{\mathbf{m}} = -j\mathbf{K} \times \hat{\mathbf{E}}^{\mathbf{m}}. \tag{16}$$

Either of these equations, coupled with (13) and (14), shows that $\hat{\mathbf{E}}^{\mathbf{m}}, \hat{\mathbf{H}}^{\mathbf{m}}$, and $\mathbf{K}$ form a mutually orthogonal set. *However*, in general $\mathbf{K}$ is not parallel to $\tilde{\mathbf{k}}$ (i.e., the direction of wave propagation). For a given discretization one can solve for $\tilde{k}$ from the dispersion relation. Given $\tilde{k}$, the components of $\mathbf{K}$ can be found via (11) and hence the angle between $\tilde{\mathbf{k}}$ and $\mathbf{K}$ can be found. The angle is, however, frequency dependent.

B. Dispersion Relation

The dispersion relation for the Yee algorithm is well established [10] and has been studied over the entire range of frequencies which can be coupled into the grid [11], [12]. The dispersion relation plays a central role in the work to follow and is derived here by solving (15) for $\hat{\mathbf{E}}^{\mathbf{m}}$ and using that to eliminate $\hat{\mathbf{E}}^{\mathbf{m}}$ from (16). The result is

$$-j\Omega\mu\hat{\mathbf{H}}^{\mathbf{m}} = -j\mathbf{K} \times \left(-\frac{1}{j\Omega\epsilon} j\mathbf{K} \times \hat{\mathbf{H}}^{\mathbf{m}}\right). \tag{17}$$

Rearranging and expanding the cross products yields

$$\Omega^2\mu\epsilon\hat{\mathbf{H}}^{\mathbf{m}} = -((\mathbf{K} \cdot \hat{\mathbf{H}}^{\mathbf{m}})\mathbf{K} - (\mathbf{K} \cdot \mathbf{K})\hat{\mathbf{H}}^{\mathbf{m}}). \tag{18}$$

From (14) $\mathbf{K} \cdot \hat{\mathbf{H}}^{\mathbf{m}}$ is zero. Since $\hat{\mathbf{H}}^{\mathbf{m}}$ appears on both sides of (18) and the equation is true for each component, it can be eliminated from (18) to obtain the dispersion relation

$$\mu\epsilon\Omega^2 = \mathbf{K} \cdot \mathbf{K} = |\mathbf{K}|^2. \tag{19}$$

In order to simplify the expressions to follow, we will assume a uniform spatial-step size so that $\delta = \Delta_x = \Delta_y = \Delta_z$ but we note that a similar approach would hold for a nonuniform grid. Expanding the terms in (19), the dispersion relation can be written in the more familiar form of

$$\frac{1}{S^2}\sin^2\left(\frac{\omega\Delta_t}{2}\right) = \sin^2\left(\frac{\tilde{k}_x\delta}{2}\right) + \sin^2\left(\frac{\tilde{k}_y\delta}{2}\right) + \sin^2\left(\frac{\tilde{k}_z\delta}{2}\right) \tag{20}$$

where S is the Courant number $c\Delta_t/\delta$.

C. Impedance

Taking the magnitude of both sides of (15) yields

$$|\Omega\epsilon\hat{\mathbf{E}}^{\mathbf{m}}| = |\mathbf{K} \times \hat{\mathbf{H}}^{\mathbf{m}}|. \tag{21}$$

Because $\mathbf{K}$ and $\hat{\mathbf{H}}^{\mathbf{m}}$ are orthogonal and all fields have the same spatial dependence, the spatial dependence can be removed leaving

$$\Omega\epsilon|\hat{\mathbf{E}}_0| = |\mathbf{K}|\,|\hat{\mathbf{H}}_0|. \tag{22}$$

Taking the square root of (19) gives the magnitude of $\mathbf{K}$ in terms of Ω, i.e., $|\mathbf{K}| = \sqrt{\mu\epsilon}\Omega$. Plugging this into (22) and rearranging yields

$$\frac{|\hat{\mathbf{E}}_0|}{|\hat{\mathbf{H}}_0|} = \frac{E_0}{H_0} = \sqrt{\frac{\mu}{\epsilon}}. \tag{23}$$

Thus the grid characteristic impedance is exact independent of the direction of propagation or discretization. However this does not imply, for instances, that the magnetic field components can be obtain in the usual manner from the electric field given the direction of propagation and polarization. Instead one must account for the lack of orthogonality as stated above (and as considered when polarization is discussed).

D. Group Velocity

The FDTD phase velocity $\tilde{c}_p$ can be obtained from the numeric wavenumber, i.e., $\tilde{c}_p = \omega/\tilde{k}$, while the grid group velocity is given by $\tilde{c}_g = \partial\omega/\partial\tilde{k}$ (the FDTD group velocity has previously been discussed in [17] and [18]). It is helpful to place bounds on both the numeric phase and group velocities. For the second-order Yee scheme, the worst dispersion occurs for grid-aligned propagation and hence closed-from bounds can be obtained (in general the multidimensional dispersion relation does not permit a closed-form solution).

For very coarsely resolved fields, the FDTD grid supports complex wave numbers which experience exponential decay [11], [12]. Although such waves should be considered in the construction of a completely exact TFSF boundary, they will be discarded in the implementation to come because : 1) owing to their exponential decay, such waves are typically of little practical concern and 2) by restricting consideration to real wavenumbers the root-finding which must be used to solve the multi-dimensional dispersion relation is greatly simplified.

For grid-aligned propagation [equivalent to discarding two of the terms on the right side of (20)] the dispersion relation can be used to solve for the ratio of the grid phase velocity to the speed of light

$$\frac{\tilde{c}_p}{c} = \frac{\pi}{N_\lambda \sin^{-1}\left(\frac{1}{S}\sin\left(\frac{\pi S}{N_\lambda}\right)\right)} \tag{24}$$

where N_λ is the number of cells per wavelength. [Here we have used $\omega\Delta_t/2 = \pi S/N_\lambda$ and $\tilde{k}\delta/2 = \pi c/(\tilde{c}_p N_\lambda)$.] The smallest discretization which yields a real wavenumber is

$$N_{\lambda,\min,r} = \frac{\pi S}{\sin^{-1}(S)}. \tag{25}$$

Using this value in (24) yields the minimum phase speed

$$\left.\frac{\tilde{c}_p}{c}\right|_{\min} = \frac{2\sin^{-1}(S)}{\pi S}. \tag{26}$$

Using the three-dimensional (3-D) Courant limit of $S = 1/\sqrt{3}$ yields a minimum phase velocity of approximately $0.6787c$.

Solving the dispersion relation for ω and calculating $\partial\omega/\partial\tilde{k}$ yields the group velocity which, when normalized by c, can be expressed as

$$\frac{\tilde{c}_g}{c} = \frac{\cos\left(\frac{\pi}{N_\lambda}\frac{c}{\tilde{c}_p}\right)}{\sqrt{1 - S^2\sin^2\left(\frac{\pi}{N_\lambda}\frac{c}{\tilde{c}_p}\right)}}. \tag{27}$$

The minimum group velocity can be found by using (25) and (26) in (27). Using these minimum values the arguments of the trigonometric functions become

$$\left.\frac{\pi}{N_{\lambda,\min,r}}\ \frac{c}{\tilde{c}_p}\right|_{\min} = \frac{\pi}{2}. \tag{28}$$

Thus, the group velocity at this discretization is identically zero! This explains why high frequency energy may persist in the FDTD grid for inordinately long times despite the fairly reasonable phase velocity: the group velocity may be very small or even zero. Fig. 1 shows a plot of the normalized phase and group velocities for grid-aligned propagation using a Courant number S of $1/\sqrt{3}$. These curves provide bounds on the worst velocity errors since obliquely propagating waves will suffer less errors. The relevance of group velocity to the TFSF boundary will be discussed below. As shown in [12], the coarsest discretization which can exist in an FDTD grid, independent of direction of propagation, is

$$N_{\lambda,\min,c} = 2S. \tag{29}$$

This can be shown by considering the highest frequency which can be coupled into the grid which is $f_{\max} = 1/(2\Delta t)$. Expressing this in terms of the shortest wavelength $\lambda_{\min}$ and the discretization one obtains $c/\lambda_{\min} = c/(N_{\lambda,\min,c}\delta)$ from which (29) follows directly.

III. TFSF Boundary

Having a complete quantification of the way in which plane waves propagate in the FDTD grid, the field at any point in the grid can be determined given an incident-field time-series at a reference point and the direction of propagation. For notational simplicity, consideration will be restricted to oblique propagation in two dimensions but the extension to three dimensions is straightforward with the one complication being polarization which will be discussed. For 3-D simulations in which the incident field propagates obliquely to two of the axes but perpendicular to the third, the derivation presented here pertains directly.

Assume one wants the incident time series to be $f[m_t]$ at the reference point $(m_{x,\mathrm{ref}}, m_{y,\mathrm{ref}})$. We take this field to correspond to the z component of the electric field in a TM_z simulation (i.e., nonzero fields are E_z, H_x, and H_y). In the frequency domain this field is given by

$$F(\omega) = \mathcal{F}(f) \tag{30}$$

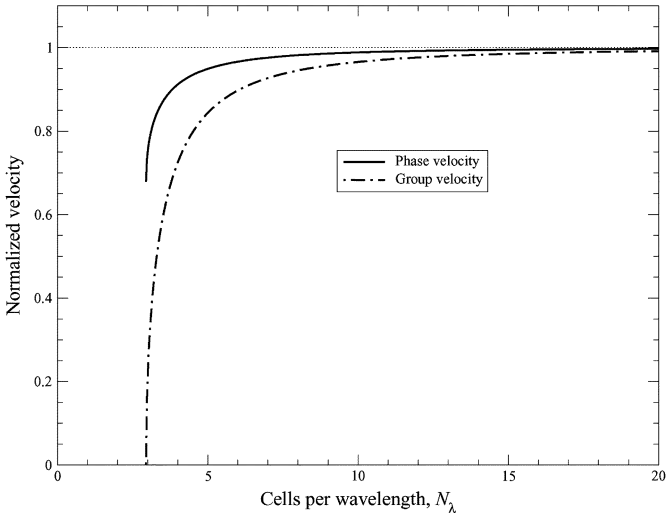

Fig. 1. Normalized phase and group velocity for grid-aligned propagation versus the discretization. The Courant number is the 3-D limit of $1/\sqrt{3}$. The coarsest discretization for which the wavenumbers are real, $N_{\lambda,\min,r}$, is approximately 2.946 97. At this discretization the group velocity goes to zero. The ideal normalized velocity is unity.

where $\mathcal{F}$ is the discrete Fourier transform. The E_z field at any other node in the grid is simply given by

$$\hat{E}_z^{\mathbf{m}} = P^{\mathbf{m}}(m_{x,\mathrm{ref}}, m_{y,\mathrm{ref}})F(\omega) \tag{31}$$

where

$$P^{\mathbf{m}}(m_{x,\mathrm{ref}}, m_{y,\mathrm{ref}}) = \exp[-j(\tilde{k}_x\delta(m_x - m_{x,\mathrm{ref}}) + \tilde{k}_y\delta(m_y - m_{y,\mathrm{ref}}))]. \tag{32}$$

$P^{\mathbf{m}}(m_{x,\mathrm{ref}}, m_{y,\mathrm{ref}})$ gives the phase shift associated with propagation from the point $(m_{x,\mathrm{ref}}, m_{y,\mathrm{ref}})$ to the arbitrary point (m_x, m_y). In the time domain the field is given by

$$E_z^{\mathbf{m}} = \mathcal{F}^{-1}(P^{\mathbf{m}}(m_{x,\mathrm{ref}}, m_{y,\mathrm{ref}})F(\omega)) \tag{33}$$

where $\mathcal{F}^{-1}$ is the inverse Fourier transform. In two dimensions one can write the x and y components of the magnetic field directly in terms of the z components of the electric field. From (16) one obtains

$$\hat{H}_x^{\mathbf{m}} = \frac{K_y}{\mu\Omega}\hat{E}_z^{\mathbf{m}} \tag{34}$$

$$\hat{H}_y^{\mathbf{m}} = -\frac{K_x}{\mu\Omega}\hat{E}_z^{\mathbf{m}}. \tag{35}$$

In the time domain these correspond to

$$H_x^{\mathbf{m}} = \mathcal{F}^{-1}\left(\frac{S\sin\left(\frac{\tilde{k}_y\delta}{2}\right)}{\eta\sin\left(\frac{\omega\Delta_t}{2}\right)}P^{\mathbf{m}}(m_{x,\mathrm{ref}}, m_{y,\mathrm{ref}})F(\omega)\right) \tag{36}$$

$$H_y^{\mathbf{m}} = -\mathcal{F}^{-1}\left(\frac{S\sin\left(\frac{\tilde{k}_x\delta}{2}\right)}{\eta\sin\left(\frac{\omega\Delta_t}{2}\right)}P^{\mathbf{m}}(m_{x,\mathrm{ref}}, m_{y,\mathrm{ref}})F(\omega)\right) \tag{37}$$

where $\eta = \sqrt{\mu/\epsilon}$. The staggering of the field components is inherently accounted for by the values of m which are not restricted to integer values (i.e., an offset of one half is used when appropriate).

Equations (33), (36), and (37) comprise the heart of the exact TFSF boundary scheme. They give the incident field at any point in the grid and are used for the incident field in the TFSF update equations as given in [2], [3]. To use this technique for an FDTD method other than the Yee method, the numeric wave numbers appropriate for that method would be used in these equations. The length of the discrete Fourier transforms will be discussed in Section IV.

For arbitrary 3-D propagation one merely has to add the third wave-vector component term to the argument of the exponential in (32) (and find six field components rather than three). Additionally one must account for the "polarization" although, as described below, there is no unique orientation for the fields since the orientation is frequency dependent.

A. Polarization

For the general 3-D problem one would have to specify a polarization in additional to giving the direction of propagation, a reference point, and the desired time series. Assume this polarization is specified by a unit vector $\mathbf{u}_P$. This vector should be chosen to be orthogonal to the direction of propagation. The direction of propagation is represented by unit vector $\mathbf{u}_{\theta\phi}$. The orientation of vector $\mathbf{K}$ is dictated by the dispersion relation and corresponds to unit vector $\mathbf{u}_K$. Note that in the limit as the discretization goes to zero $\mathbf{u}_{\theta\phi}$ and $\mathbf{u}_K$ will be parallel.

The orientation of the magnetic field can now be specified by

$$\mathbf{u}_H = \mathbf{u}_K \times \mathbf{u}_P. \tag{38}$$

Knowing the impedance in the grid is exact, one can obtain the magnetic field components from the scalar incident electric field as

$$\hat{\mathbf{H}}^{\mathbf{m}} = \sqrt{\frac{\epsilon}{\mu}}\hat{E}^{\mathbf{m}}(\mathbf{u}_K \times \mathbf{u}_P). \tag{39}$$

With the orientations of $\mathbf{K}$ and $\hat{\mathbf{H}}^{\mathbf{m}}$ now fixed, the orientation of the electric field is fixed by the orthogonality condition given in Section II-A. Thus

$$\hat{\mathbf{E}}^{\mathbf{m}} = \hat{E}^{\mathbf{m}}(\mathbf{u}_H \times \mathbf{u}_K) \tag{40}$$

$$= \hat{E}^{\mathbf{m}}(\mathbf{u}_P - [\mathbf{u}_K \cdot \mathbf{u}_P]\mathbf{u}_K) \tag{41}$$

where the second equation is obtained by substituting (38) into the first. As mentioned, $\mathbf{u}_K$ is parallel to the direction of propagation in the limit of small discretization. Since the polarization $\mathbf{u}_P$ is chosen to be orthogonal to the direction of propagation, the term in brackets in (41) goes to zero in this limit leaving $\hat{\mathbf{E}}^{\mathbf{m}} = \hat{E}^{\mathbf{m}}\mathbf{u}_P$. Thus in the limit, the electric field is oriented with the desired polarization.

B. Delay

It is possible to have the reference point interior to the TF region as shown in Fig. 2. In the implementations used by the author, one specifies a time series starting at time zero without regard to the reference location. The transforms are then done in such a way as to ensure the field at the reference point will take on the values of the specified time series. However, unless the reference point was at one of the corners of the TFSF boundary, the fields have to propagate to the reference point and hence they will be delayed. To determine the amount of delay, the distance the fields have to travel is divided by the speed of propagation. However this speed must be the group velocity, not the phase velocity. As stated previously, the group velocity goes to zero at the coarsest discretization supported by the grid (at the lower bound of grid-aligned propagation). This would indicate an infinite delay. However, such coarsely discretized components are typically not of practical interest and hence a delay based on the group velocity at a discretization that is some small multiple ξ of $N_{\lambda,\min,r}$ is used to calculate the delay (the code written thus far uses an ξ of $9/8$).

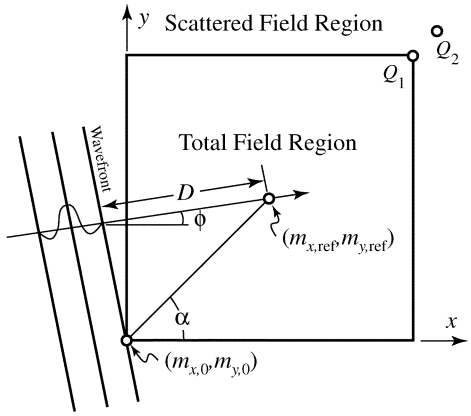

Fig. 2. Placement of the reference point interior to the total-field region. The plane wave must propagate over a distance D before reaching the reference point. The angle α is between the x axis and a line from the lower-left corner to the reference point. The incident wave is assumed to propagate at an angle ϕ with respect to the x axis. The point Q_1 corresponds to the upper right corner while Q_2 is slightly above and to the right of the TF region.

From Fig. 2 the distance from the reference point to a phase front collocated with the lower-left corner is defined to be D and given in number of cells $N_D = D/\delta$ by

$$N_D = \cos(\alpha - \phi)[(m_{x,0} - m_{x,\mathrm{ref}})^2 - (m_{y,0} - m_{y,\mathrm{ref}})^2]^{1/2} \tag{42}$$

where α is the angle between the x axis and a line from the lower-left corner to the reference point, and ϕ is the direction of propagation. The delay (or time) associated with propagation over this distance is, to be conservative, calculated using the grid-aligned group velocity and a discretization of $\xi N_{\lambda,\min,r}$. The result in terms of time steps is

$$N_t = \frac{N_D}{S}\frac{\sqrt{1 - \sin^2\left(\frac{1}{\xi}\sin^{-1}(S)\right)}}{\cos\left(\sin^{-1}\left[\frac{1}{S}\sin\left(\frac{1}{\xi}\sin^{-1}(S)\right)\right]\right)}. \tag{43}$$

(This is obtained by dividing the distance N_D by the group velocity (27) using a discretization $\xi N_{\lambda,\min,r}$). Instead of taking the Fourier transform of $f[m_t]$ one would take the transform of the delayed function $f[m_t - N_t]$.

Note that delay is only of interest when the reference point is not a corner of the TFSF boundary. This provides the rather novel ability to ensure the time series at a given interior point is as specified (albeit with some small errors), but if one does not have the need for such behavior it would be best to make the reference point correspond to one of the corners.

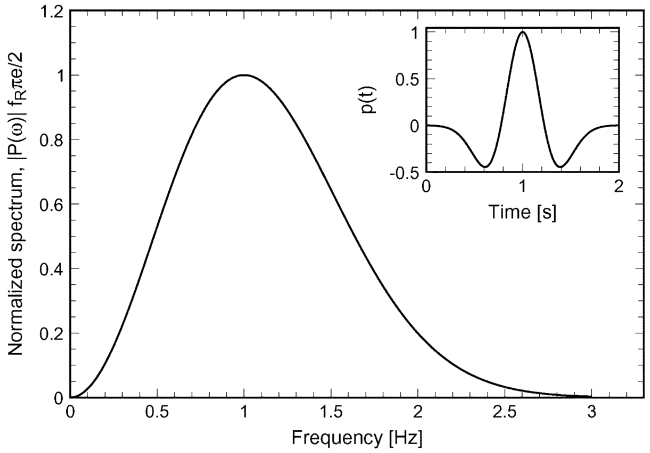

Fig. 3. Normalized spectrum of the Ricker wavelet where the most energetic frequency f_R is 1 Hz. The inset shows the time-domain form with a delay of $1/f_R$. Changes of f_R rescale the horizontal scales but do not change the fundamental shapes of the curves.

IV. Results

The incident pulse is assumed to be a Ricker wavelet which corresponds to the second derivative of a Gaussian (but note any incident pulse is permitted). We define the most energetic frequency of the pulse to be f_R and the discretization at this frequency to be N_R cells per wavelength. The time-series form of the wavelet is

$$f[m_t] = \left(1 - 2\pi^2 \left(\frac{Sm_t}{N_R} - 1\right)^2\right) \exp\left[-\pi \left(\frac{Sm_t}{N_R} - 1\right)^2\right]. \tag{44}$$

The negative ones correspond to a delay of the pulse such that the peak will occur at a time $t = 1/f_R$ or in discretized form at a time step $m_t = N_R/S$ (notwithstanding that this may not be an integer value). A plot of the Ricker wavelet spectrum is shown in Fig. 3 which also shows the time-domain form as an inset plot. The plot shows the wavelet for an f_R of 1 Hz. Were one interested in a different f_R the horizontal axes would be scaled according (with unity corresponding to f_R in the spectral plot and unity corresponding to $1/f_R$ in the temporal plot), but the shape of the curves would be unchanged. Note that if the Ricker wavelet has its most energetic frequency f_R at 10 cells per wavelength, there is still significant energy present at $2f_R$ (5 cells per wavelength) and even nonvanishing energy at $2.5f_R$ (4 cells per wavelength) and beyond. Thus one anticipates a pulse discretized in such a way would, in general, suffer a great deal of dispersion. Since the goal of this section is to demonstrate the capabilities of the exact TFSF formulation, using such a poorly discretized pulse is ideal.

To illustrate how the selection of the reference point affects the fields, we plot the electric field at three points interior to a 2-D TF region which is 102×102 cells^2. The three points are indicated in Fig. 2 and correspond to the lower-left corner, the center, and the upper right corner (labeled Q_1). The Courant number is $1/\sqrt{3}$ (so the fields associated with this simulation could pertain to a 3-D simulation) and the Ricker wavelet is discretized with 10 cells per wavelength at its most energetic frequency. The incident field is propagating at 30° relative to the

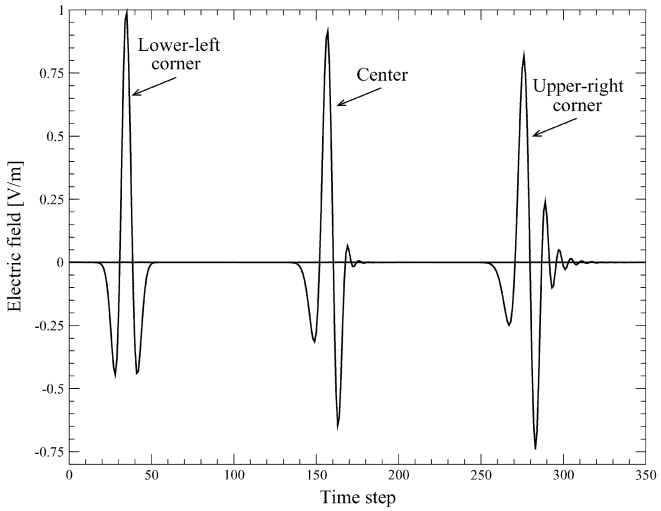

Fig. 4. Electric field versus time step at the lower-left corner, center, and upper-right corner of the TF region. Incident field is a Ricker wavelet discretized at 10 cells per wavelength at its most energetic frequency and the Courant number is $1/\sqrt{3}$. Here the reference point is the lower-left corner.

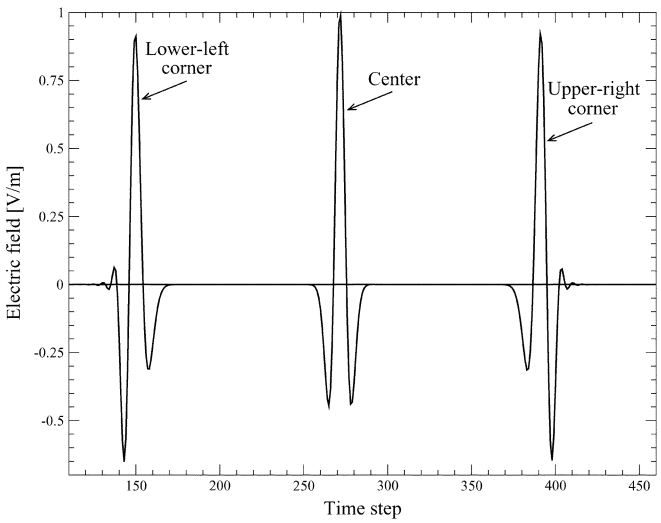

Fig. 5. Same as Fig. 4 except the reference point has been moved to the center of the TF region.

x axis. Fig. 4 shows the electric field at these points as a function of the time step when the reference point is the lower-left corner. Note that the field at the lower-left corner corresponds to the given sampled version of the Ricker wavelet. At the center, owing to the rather coarse discretization being used, the effects of dispersion have clearly distorted the pulse. These effects are even more clearly pronounced when the field reaches the upper right corner. The amount of leakage into the scattered-field region will be considered shortly.

Fig. 5 shows the electric field at the same three points when the reference point is at the center of the computational domain. The same time series was supplied to the program which generated the results for both Figs. 4 and 5—only the reference point was change. As described in Section III-B, the program calculated an appropriate delay when the reference point was moved from the corner. The leading time-steps which had exceedingly small field values are not shown in Fig. 5. Note that the field in the lower-left corner now is distorted—the leading

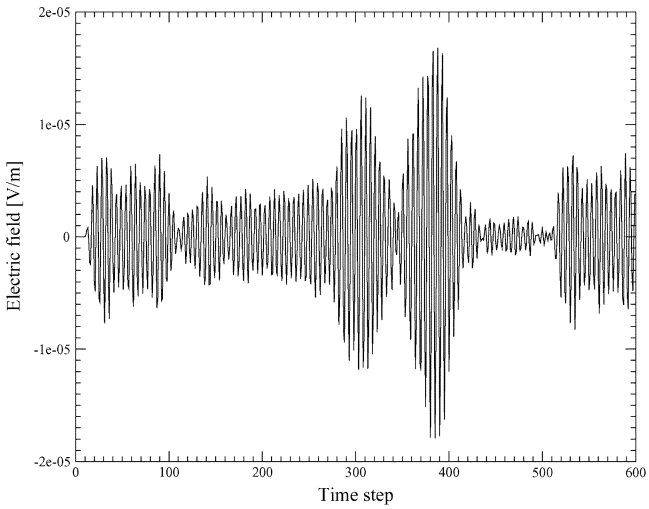

Fig. 6. Field leaked into the scattered-field region (point Q_2) using a Ricker wavelet discretized at 10 cells per wavelength at the most energetic frequency. The leakage is essentially 100 dB down from the peak value of the incident field.

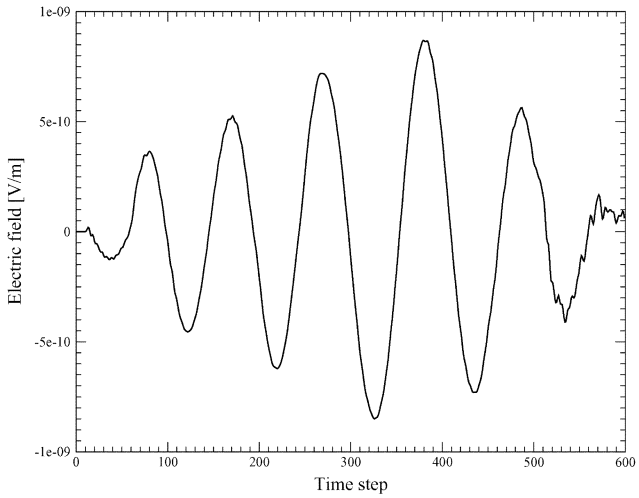

Fig. 7. Field leaked into the scattered-field region (point Q_2) using a Ricker wavelet discretized at 20 cells per wavelength at the most energetic frequency. The leakage is less than 180 dB down from the peak incident field.

field corresponds to the coarsely discretized components of the pulse. Since these components propagate more slowly than the more finely discretized components, they must be introduced into the grid first if the field at the reference point is to be correct. Fig. 5 does show that the field at the reference point now corresponds to an undistorted Ricker pulse. The field at the upper-right corner is distorted but by an amount commensurate with what was seen at the center point in Fig. 4.

To demonstrate the level of accuracy that can be expected with the TFSF boundary proposed here, the field at a point five cells to the right and five cells above the upper-right corner of the TF region is recorded. This point is shown as Q_2 in Fig. 2. The incident field is as described above with the reference point in the lower-left corner. The measured field is shown in Fig. 6. The peak amplitude of the incident pulse is unity so these "leaked fields" are typically more than 100 dB down from the peak value. Fig. 7 shows the field at the same point and with the same incident field except now the Ricker wavelet has been discretized such that there are 20 cells per wavelength at the most energetic frequency. Here the leaked fields are more than 180 dB down from the peak value of the incident field. These error levels are such that in nearly all practical simulations one can be assured the dominant error is caused by something other than the TFSF boundary. For these simulations the total computational domain was 141×141 cells^2 and no absorbing boundary conditions were implemented (hence any energy leaked into the SF region will persist). In both Figs. 6 and 7 some acausal energy is observed at the scattered field point. This is caused by the truncation in the Fourier transforms. Were the Fourier transform to be performed with all wavenumbers (real and complex), the field would effectively be causal (i.e., zero in the scattered field region except for errors caused by the wavenumber root-finding and numerical errors inherent in the finite precision of the floating-point numbers used).

Note that Figs. 6 and 7 show time out to 600 time steps. However the TFSF code only calculated the incident field to 500 steps at which point the incident field was effectively declared zero (one should keep in mind group velocity rather than phase velocity when determining the time needed for the incident field to traverse the TF region). An FDTD simulation can be run to any number of time steps and yet this does not require that the TFSF code calculate the incident field beyond the time it is effectively zero over the TFSF boundary. Since the incident field was only needed for 500 time steps, the Fourier transforms were performed using a 512-point fast Fourier transform (FFT). The length of the FFT must be sufficiently long to contain the entire incident time series but need not be longer (in this case after performing the inverse FFT 12 points were discarded).

One of the reasons errors are still present in these simulation is that all wavenumbers whose discretizations are less than $N_{\lambda,\min,r}$ are discarded (i.e., in the interest of avoiding complex root-finding, all wavenumbers are guaranteed to be real if one discards those with discretizations in the range from $N_{\lambda,\min,c}$ to $N_{\lambda,\min,r}$). Since $N_{\lambda,\min,r}$ was determined under the assumption of grid-aligned propagation, for obliquely propagating waves there will be some discretizations less than $N_{\lambda,\min,r}$ which yield real wavenumbers. By discarding them the energy associated with those components is lost and this introduced some error. Another source of error is introduced by using root-finding (Newton's method was used) to solve the dispersion equation since it lacks a closed-form solution.

Programs to realize this TFSF boundary can be found in the code section of the Web site www.fdtd.org or can be obtained by contacting the author. The programs are written in C and can either produce an incident-field file or can be incorporated directly into a program. The user specifies such things as the time series (actually a function which can be called to obtain the time series), a reference point, the Courant number, the impedance, the direction of propagation, and the desired number of time steps. The incident field is calculated and a function is supplied which applies these fields to nodes adjacent to the TFSF boundary. All calculations are in double precision. The FFTs are performed using the FFTw routines noted in the Introduction. For the examples presented here, which required the calculation of roughly 816 FFTs of 512 points, the computation time was roughly 0.11 s on a 2 GHz Apple G5 running OS X 10.3.

V. Conclusion

Since it is possible to quantify exactly how a plane wave propagates in the Yee FDTD grid, it is possible to calculate the time series at an arbitrary point given the incident field at a reference point and the direction of propagation. This allows one to realize an exact TFSF boundary for arbitrary directions of propagation. For the sake of implementation simplicity, only waves with real wavenumbers were considered. This provides nearly 180 dB of accuracy for reasonably discretized waves, essentially ensuring any errors present in a simulation are dominated by something other than the TFSF implementation. Were one to desire additional accuracy, a complex root-finding algorithm could be employed to quantify the behavior of all field components down to the coarsest discretization which can exist in the grid. The TFSF implementation described here lacks some of the simplicity of alternative 1-D auxiliary-grid approaches, but the code necessary to realize the implementation was straightforward to write, is relatively fast, and has been made available to the public under the GNU General Public License.

References

[1] D. E. Merewether, R. Fisher, and F. W. Smith, "On implementing a numeric Huygen's source scheme in a finite difference program to illuminate scattering bodies," *IEEE Trans. Nucl. Sci.*, vol. 27, no. 6, pp. 1829–1833, Dec. 1980.

[2] A. Taflove, *Computational Electrodynamics: The Finite-Difference Time-Domain Method*. Boston, MA: Artech House, 1995.

[3] A. Taflove and S. Hagness, *Computational Electrodynamics: The Finite-Difference Time-Domain Method*, 2nd ed. Boston, MA: Artech House, 2000.

[4] K. S. Yee, "Numerical solution of initial boundary value problems involving Maxwell's equations in isotropic media," *IEEE Trans. Antennas Propagat.*, vol. 14, no. 3, pp. 302–307, Mar. 1966.

[5] V. Anantha and A. Taflove, "Efficient modeling of infinite scatterers using a generalized total-field/scattered-field FDTD boundary partially embedded within PML," *IEEE Trans. Antennas Propagat.*, vol. 50, no. 10, pp. 1337–1349, Oct. 2002.

[6] K. Demarest, R. Plumb, and Z. Huang, "FDTD modeling of scatterers in stratified media," *IEEE Trans. Antennas Propagat.*, vol. 43, no. 10, pp. 1164–1168, Oct. 1995.

[7] C. Guiffaut and K. Mahdjoubi, "Perfect wideband plane wave injector for FDTD method," in *Proc. IEEE Antennas Propagat. Soc. Int. Symp.*, vol. 1, Salt Lake City, UT, July 2000, pp. 236–239.

[8] U. Oğuz and L. Gürel, "Interpolation techniques to improve the accuracy of the plane wave excitations in the finite difference time domain method," *Radio Sci.*, vol. 32, no. 6, pp. 2189–2199, Nov.–Dec. 1997.

[9] ——, "An efficient and accurate technique for the incident-wave excitations in the FDTD method," *IEEE Trans. Microwave Theory and Techniques*, vol. 46, no. 6, pp. 869–882, June 1998.

[10] A. Taflove, "Review of the formulation and applications of the finite-difference time-domain method for numerical modeling of electromagnetic wave interactions with arbitrary structures," *Wave Motion*, vol. 10, no. 6, pp. 547–582, 1988.

[11] J. B. Schneider and C. L. Wagner, "FDTD dispersion revisited: Faster-than-light propagation," *IEEE Microwave Guided Wave Lett.*, vol. 9, no. 2, pp. 54–56, Feb. 1999.

[12] J. B. Schneider and R. J. Kruhlak, "Dispersion of homogeneous and inhomogeneous waves in the Yee finite-difference time-domain grid," *IEEE Trans. Microwave Theory and Techniques*, vol. 49, no. 2, pp. 280–287, Feb. 2001.

[13] ——, "Plane waves and planar boundaries in FDTD simulations," in *Proc. IEEE Antennas and Propagat. Soc. Int. Symp. URSI Radio Sci. Meeting*, Salt Lake City, UT, July 2000.

[14] M. Celuch-Marcysiak and W. K. Gwarek, "On the nature of solutions produced by finite difference schemes in time domain," *Int. J. Numerical Modeling: Electronic Networks, Devices, and Fields*, vol. 12, no. 1–2, pp. 23–40, Jan.–Apr. 1999.

[15] M. Frigo and S. G. Johnson, "FFTW: An adaptive software architecture for the FFT," in *Proc. Int. Conf. Acoustics, Speech, and Signal Processing*, vol. 3, 1998.

[16] E. A. Forgy, "A Time-domain method for computational electromagnetics with isotropic numerical dispersion on an overlapped latice," Master's thesis, University of Illinois at Urbana-Champaign, Urbana-Champaign, IL, 1998.

[17] L. N. Trefethen, "Group velocity in finite difference schemes," in *SIAM Rev.*, vol. 24, 1982, pp. 113–135.

[18] D. H. Choi and J. E. Roy, "The dispersion characteristics of the FD-TD method," in *Proc. IEEE Antennas Propagat. Soc. Int. Symp.*, San Jose, CA, 1989, pp. 26–29.

John B. Schneider (M'00) received the B.S. degree in electrical engineering from Tulane University, New Orleans, LA, and the M.S. and Ph.D. degrees in electrical engineering from the University of Washington, Seattle.

He is presently an Associate Professor in the School of Electrical Engineering and Computer Science, Washington State University, Pullman. His research interests include the use of computational methods to analyze acoustic, elastic, and electromagnetic wave propagation.